Whither the 100th Meridian? The Once and Future Physical and Human Geography of America's Arid–Humid Divide. Part II: The Meridian Moves East

Richard Seager[a]

Lamont-Doherty Earth Observatory, Columbia University, Palisades, New York

Jamie Feldman

School of Engineering and Applied Sciences, Columbia University, New York, New York

Nathan Lis

Department of Meteorology and Atmospheric Science, The Pennsylvania State University, University Park, Pennsylvania

Mingfang Ting, Alton P. Williams, Jennifer Nakamura, Haibo Liu, and Naomi Henderson

Lamont-Doherty Earth Observatory, Columbia University, Palisades, New York

[a]*Corresponding author*: Richard Seager, seager@ldeo.columbia.edu

ABSTRACT: The 100th meridian bisects the Great Plains of the United States and effectively divides the continent into more arid western and less arid eastern halves and is well expressed in terms of vegetation, land hydrology, crops, and the farm economy. Here, it is considered how this arid–humid divide will change in intensity and location during the current century under rising greenhouse gases. It is first shown that state-of-the-art climate models from phase 5 of the Coupled Model Intercomparison Project generally underestimate the degree of aridity of the United States and simulate an arid–humid divide that is too diffuse. These biases are traced to excessive precipitation and evapotranspiration and inadequate blocking of eastward moisture flux by the Pacific coastal ranges and Rockies. Bias-corrected future projections are developed that modify observationally based measures of aridity by the model-projected fractional changes in aridity. Aridity increases across the United States, and the aridity gradient weakens. The main contributor to the changes is rising potential evapotranspiration, while changes in precipitation working alone increase aridity across the southern and decrease across the northern United States. The "effective 100th meridian" moves to the east as the century progresses. In the current farm economy, farm size and percent of county under rangelands increase and percent of cropland under corn decreases as aridity increases. Statistical relations between these quantities and the bias-corrected aridity projections suggest that, all else being equal (which it will not be), adjustment to changing environmental conditions would cause farm size and rangeland area to increase across the plains and percent of cropland under corn to decrease in the northern plains as the century advances.

KEYWORDS: North America; Vegetation–atmosphere interactions; Hydrometeorology; Agriculture

1. Introduction

The 100th meridian was conceptualized by the nineteenth-century explorer, scientist, and director of the U.S. Geological Survey and Bureau of Ethnology John Wesley Powell as the clearly demarcated divide between America's arid west and humid east (Powell 1879, 1890). In Part I of this two-part paper, we showed the validity of this conceptual divide in terms of a sharp zonal gradient in aridity across the Great Plains, elucidated the physical processes in the atmosphere that establish the aridity gradient, and examined how it is expressed in terms of land surface hydrology and vegetation and, finally, how it is realized in terms of the agricultural economy. It was found that, on all scores, the 100th meridian does indeed represent a divide in the physical character and social and economic structure of the central United States. Powell used the 100th meridian to argue that plans for settlement and development of the arid land west of the meridian should be different to those applied to the East and be very conscious of the constraints imposed by aridity and the need for irrigation in the presence of limited water availability. While his ideas were largely ignored (Stegner 1954), apparently it is nonetheless the case that environmental conditions did influence the land development and use over the period since Powell.

The 100th meridian as the arid–humid divide was a description of the late-nineteenth-century climate and landscape that has remained valid at least into the beginning of this century. But now climate change caused by rising greenhouse gases from fossil fuel burning is advancing. Based on the most recent climate model projections from phase 5 of the Coupled Model Intercomparison Project (CMIP5) and analyzed by the Intergovernmental Panel on Climate Change (IPCC) Fifth Assessment

Report (AR5), many workers have reported that North America will see, over the coming decades, a marked transition in hydroclimate. Precipitation is expected to decline in southwestern North America but increase in the northeast, and temperature will rise everywhere (Seager et al. 2013; Maloney et al. 2014; Seager et al. 2014). Cook et al. (2015) used the CMIP5 model ensemble to show that these changes combine to cause a quite alarming increase in aridity in the plains as measured either by the Palmer drought severity index (utilizing the Penman–Monteith formulation for potential evapotranspiration) or in the actual modeled soil moisture. Under such climate change we would expect the modeled arid–humid divide to move or the "effective 100th meridian" to advance eastward. Given that the aridity gradient is expressed in the agricultural economy, this could necessitate farms to adapt to new environmental conditions, by consolidation and changes in crops grown, for example, or risk becoming unprofitable. Disruption could be minimized if the climate changes and agricultural economic implications were anticipated in advance.

To project the future we need models. These can range greatly in complexity, but for future climate change the best guidance comes from the coupled atmosphere–ocean–land–sea ice models of the CMIP5. Here in Part II, we will use the CMIP5 models to compute projections of the change in aridity and aridity gradient for the next century. However, we should never use these models blindly, and instead we should be fully aware of model biases and limitations. Often a "bias correction" is needed and one will be applied here to estimate the future aridity index. We will then use simple relations between aspects of the agricultural economy and the aridity index to suggest the implications of the changes in climate. The work suggests that the 100th meridian in effect moves steadily east. The physical reasons for why this is so will be determined. The implications are that, all else being equal (which it will not be), cultivation of wheat and rangelands will expand east at the expense of corn and that farm size will need to increase to reflect the new climate and land productivity.

2. Observational and climate model data

To compare the models against observations, we use data from the National Land Data Assimilation System 2 (NLDAS-2). The following text follows that in Part I. NLDAS-2 is a land surface model based on land surface hydrology models driven by atmospheric data (Xia et al. 2012a,b) available online (at http://ldas.gsfc.nasa.gov/index.php; last accessed September 2017). Land surface models are physical models of the upper part of the land surface that solve equations for transfer of heat and moisture between the surface and the deeper layers and that also contain a representation of vegetation and interactions between it, the atmosphere, and the soil below. The land surface models are forced by imposed air temperature, humidity, winds, surface radiation, and other quantities. In this case atmospheric data from the National Centers for Environmental Prediction (NCEP) North American Regional Reanalysis (NARR) reanalysis (Mesinger et al. 2006) are used in combination with precipitation data developed by the PRISM Climate Group at Oregon State University [details of which can be found at http://www.prism.oregonstate.edu and in Daly et al. (2000)]. The data period covers 1979 to 2015, and the spatial resolution is $\frac{1}{8}°$ in latitude and longitude. The atmospheric data were used by NLDAS-2 to force three different land surface models, Mosaic, VIC, and Noah, but, for brevity, as in Part I, we only present results using the Noah model. For farm economy we examined type of

agricultural use, crops grown, and farm numbers and size using the USDA/National Agriculture Statistics Service 2012 Census of Agriculture data at the county level (www.agcensus.usda.gov/Publications/2012/Online_Resources/Ag_Census_Web_Maps/Overview; last accessed 30 September 2017). For nonfederal rangelands, defined as grasslands that provide forage for grazing animals, we used data from the USDA Natural Resources Conservation Service (available at https://www.nrcs.usda.gov/wps/portal/nrcs/detail/national/technical/nra/nri/?cid=stelprdb1253602; last accessed 30 September 2017). This provides rangeland area in hectares, which we convert to the percent of rangeland for each U.S. county.

To analyze precipitation, evapotranspiration, and atmospheric moisture transports, we make use of the European Centre for Medium-Range Weather Forecasts (ECMWF) ERA-Interim for the 1979 to 2015 period (Dee et al. 2011). ERA-Interim assimilates multiple sources of atmospheric and surface data into a recent version of ECMWF's weather forecast model using up-to-date data assimilation methods. Notably, it assimilates satellite-derived, moisture-sensitive irradiances and pays close attention to representing the hydrological cycle. The moisture transports within the ERA-Interim will be compared to those from the climate models.

We make use of all the models that participated in CMIP5 that provide all the data needed. The need for 6-hourly data to evaluate moisture transports limits the number of models to 18. We use one run from each of the models. The models and some of their details are given in Table 1. To compare model simulations to the observed state, we analyze the "historical" coupled simulations forced by known and estimated changes in radiative forcing, land use, etc., for 1979 to 2005 and the RCP8.5 business-as-usual projections of the 2006 to 2100 period forced by estimates of changes in climate forcing, assuming no effort is made to reduce greenhouse gas emissions. This scenario is chosen because of the current lack of any enforceable and strong international agreement to combat climate change. All model data were regridded to a common $2° \times 2°$ grid. The numerical methods for evaluating moisture transport in the models and ERA-Interim are as in Seager and Henderson (2013), and computations were done on 6-hourly data. Computations are first done for each model run before averaging in time for each model, as needed, and then across the models to create the multimodel means shown here.

3. Methodology for projecting future aridity and impact on agricultural economy

3.1. Future AI projections

The aridity index (AI), which equals precipitation P as a fraction of potential evapotranspiration PET, $AI = P/\text{PET}$, was defined in Part I, where we evaluated it using monthly data from the observationally based NLDAS-2. Here, we will use data from both NLDAS-2 and from the CMIP5 models and compute AI for both based on monthly data. AI is evaluated using seasonal means of P and PET. For the models we have the simulations of the historical period and the projections of the future. Hence, using subscripts h and f to refer to historical and future and N to refer to NLDAS-2, we have $AI_{N,h} = P_{N,h}/\text{PET}_{N,h}$. Similarly for the CMIP5 models, denoted by subscript C, we have $AI_{C,h} = P_{C,h}/\text{PET}_{C,h}$ and $AI_{C,f} = P_{C,f}/\text{PET}_{C,f}$. PET for both NLDAS and CMIP5 is computed using the Food and Agriculture

Table 1. CMIP5 models used in this study, their ensemble size, institution, and horizontal and vertical resolution.

Model	Ensemble size	Institute	Resolution (lat × lon), level
1. BCC_CSM1.1	1	Beijing Climate Center, China	T42 (2.77°× 2.81°), L26
2. BCC_CSM1.1(m)	1	Meteorological Administration	T106, L26
3. BNU-ESM	1	College of Global Change and Earth System Science, Beijing Normal University (BNU)	T42, L26
4. CanESM2	5	Canadian Centre for Climate Modeling and Analysis (CCCma)	T63 (1.875° × 1.875°), L35
5. CNRM-CM5	5	Centre National de Recherches Météorologiques Centre Européen de Recherche et de Formation Avancée en Calcul Scientifique (CNRM-CERFACS)	T127(1.4° × 1.4°), L31
6. CSIRO Mk3.6.0	10	Commonwealth Scientific and Industrial Research Organisation in collaboration with the Queensland Climate Change Centre of Excellence (CSIRO-QCCCE)	T63(1.875° × 1.875°), L18
7. GFDL CM3	1	Geophysical Fluid Dynamics	C48 (2.0° × 2.5°), L48
8. GFDL-ESM2G	1	Laboratory (NOAA GFDL)	2.0° × 2.5°, L24
9. GFDL-ESM2M	1		2.0° × 2.5°, L24
10. HadGEM2-CC	1	Met Office Hadley Centre	N96, L38
11. INM-CM4.0	1	Institute for Numerical Mathematics (INM)	1.5° × 2.0°, L21
12. IPSL-CM5A-LR	4	Institut Pierre-Simon Laplace (IPSL)	1.875° × 3.75°, L39
13. IPSL-CM5A-MR	1		1.25° × 2.5°, L39
14. IPSL-CM5B-LR	1		1.875° × 3.75°, L39
15. MIROC5	3	Atmosphere and Ocean Research	T85, L40
16. MIROC-ESM	1	Institute (University of Tokyo),	T42, L80
17. MIROC-ESM-CHEM	1	National Institute for Environmental Studies, and Japan Agency for Marine-Earth Science and Technology (AORI/NIES/JAMSTEC)	T42, L80
18. MRI-CGCM3	1	Meteorological Research Institute (MRI)	TL159 (1.125° × 1.125°), L48

Organization version of the Penman–Monteith equation (see Allen et al. 1998). This is given by briefly dropping the N and C subscripts:

$$\text{PET}_h = \frac{0.408\Delta(R_{n,h} - G) + \gamma\frac{900}{T_{a,h} + 273}u_{2,h}(e_{s,h} - e_{a,h})}{\Delta + \gamma(1 + 0.34u_{2,h})}, \tag{1}$$

$$\text{PET}_f = \frac{0.408\Delta(R_{n,f} - G) + \gamma\frac{900}{T_{a,f} + 273}u_{2,f}(e_{s,f} - e_{a,f})}{\Delta + \gamma(1 + 0.34u_{2,f})}, \tag{2}$$

where the variables for $R_n, G, T_a, u_2, e_s, e_a$ are taken from NLDAS-2 or CMIP5. The term R_n is net surface radiation, G is ground heat flux (unavailable for the

models and set to zero), T_a is air temperature, u_2 is wind speed above the surface, e_s is the saturation vapor pressure at T_a and e_a is the actual vapor pressure (both in mb), Δ is the slope of the saturation vapor pressure curve with temperature, and γ is the psychrometric constant. Unlike for NLDAS-2, we found that for some models it was necessary to set a minimum vapor pressure deficit $VPD = e_s - e_a$ in order to prevent very small or negative PET and extreme large and/or negative values of AI. A minimum value of 0.1 mb (considerably less than typical minimum winter values of 1 mb or more) was imposed.

As we shall see, $AI_{C,h}$, the CMIP5 model AI for the historical period, has significant biases compared to that from NLDAS-2 $AI_{N,h}$, including a much weaker zonal gradient. To examine future changes in the AI, we wish to preserve the spatial features of the observed historical period and hence adopt a bias correction methodology. We will use the CMIP5 models to evaluate the fractional change in AI at each latitude and longitude and then adjust the long-term 1979–2015 climatological NLDAS-2 AI, denoted by $\overline{AI}_{N,h}$, by the CMIP5 modeled fraction. Hence, for each season, year, and model, we compute

$$\alpha_{P,\text{PET}} = AI_{C,f}/AI_{C,h}. \tag{3}$$

Here, the subscript P, PET indicates that this fraction is evaluated allowing for all climate information to vary from the historical period to the future. Next, we evaluate

$$AI_{N,f} = \alpha_{P,\text{PET}} \times \overline{AI}_{N,h}. \tag{4}$$

This then is the bias-corrected AI projection, based on both NLDAS-2 and the CMIP5 models, allowing for all climate to change. The term $AI_{N,f}$ was evaluated for each season and year from 2016 to 2100 for each model. The results are shown for the multimodel average.

It is of interest to determine the physical causes of the change in AI. To do this we compute projections of AI, allowing P and PET to change one at a time. For this, we define $AI_{C,f,P}$ as the model AI for the future, allowing only P to change and keeping PET at historical values, and $AI_{C,f,\text{PET}}$ as the model AI for the future, allowing only PET to change and keeping P at historical values. These are

$$AI_{C,f,P} = P_f/\text{PET}_h \quad \text{and} \tag{5}$$

$$AI_{C,f,\text{PET}} = P_h/\text{PET}_f. \tag{6}$$

Next, for each season, year, and model, we compute fractional changes α_P and α_{PET} that arise from P and PET change, each in isolation:

$$\alpha_P = AI_{C,f,P}/AI_{C,h} \quad \text{and} \tag{7}$$

$$\alpha_{\text{PET}} = AI_{C,f,\text{PET}}/AI_{C,h}. \tag{8}$$

We can then apply these fractional changes to the NLDAS-2 AI to derive bias-corrected AI projections:

$$\mathrm{AI}_{N,f,P} = \alpha_P \times \overline{\mathrm{AI}}_{N,h} \quad \text{and} \tag{9}$$

$$\mathrm{AI}_{N,f,\mathrm{PET}} = \alpha_{\mathrm{PET}} \times \overline{\mathrm{AI}}_{N,h}. \tag{10}$$

These are the future AI if only *P* or PET changed in isolation to be compared to when they all change together $\mathrm{AI}_{N,f}$.

3.2. Evaluating plausible impacts of future aridity on the agricultural economy

In Part I, we showed using maps that there was a notable west–east gradient in farm size and rangeland coverage, at all latitudes, and percent of cropland under wheat or corn, in the northern plains, that was associated with the aridity gradient. To examine how changes in AI will impact the agricultural economy we will first use the historical data to examine farm size, rangeland coverage, and percent of crops under corn as a function of the AI. This will be done separately for the southern, central, and northern plains, with the expectation that we will see different relationships. We will then fit polynomials to the data distributions. We will then use the future bias-corrected AI projections and the polynomial relations developed on observed historical data to project future farm size, rangeland coverage, and percent of crops under corn. For the historical relations it is reasonable to suppose that they reflect an adjustment of the farm economy to prevailing environmental conditions. The projections therefore simply assume that the future farm economy will undergo a similar adjustment to changing environmental conditions and ignore other changes (technological change, economic adjustment, subsidies, etc.) that could also be influential. Our goal here is to provide a simple illustration of plausible change and not a prediction of actual expected change, which will additionally be affected by other factors such as changes in technology and plant water-use efficiency caused by CO_2 fertilization.

4. Results

4.1. The 100th meridian in state-of-the-art climate models

We begin by examining how well the current generation of climate models (those participating in CMIP5) simulate *P*, PET, and the AI. Figure 1 shows these by season for the multimodel average across the CMIP5 models, and Figure 2 shows annual-mean values and, for comparison, those from NLDAS-2. The precipitation distribution, with the wettest conditions in the Pacific Northwest and southeast in winter and spring and drier conditions in the southwest and interior west year-round, is qualitatively correct. Also qualitatively correct is the more zonal pattern of PET with declining values from south to north and the development of high PET regions in the southwest and southern plains in summer. The model AI shows vast areas of highly positive values in the northwest and east during fall and winter separated by a central region of lower values that spreads into the southwest and widespread values less than 1 in the spring and summer with minimum values in the southwest.
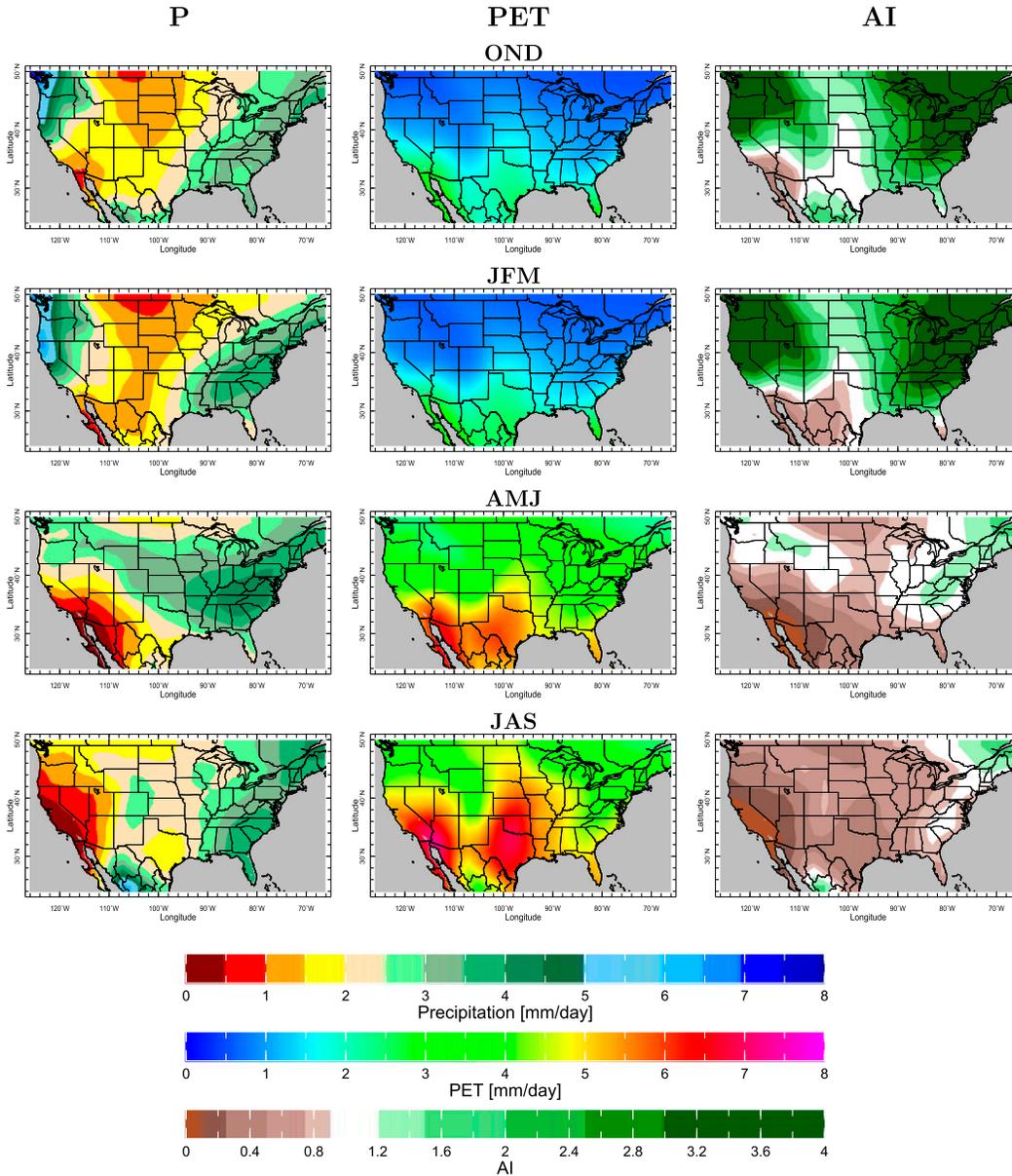
Figure 1. Parameters *P*, PET, and AI by season for (top to bottom) October–December (OND), January–March (JFM), April–June (AMJ), and July–September (JAS) for the average across the CMIP5 models for the historical period. Units for *P* and PET are mm day^{-1}.

Comparing the annual-mean *P*, PET, and AI to those derived from NLDAS-2 (Figure 2), it is clear the models fail to simulate the stark west–east AI gradient across the plains. In the central and northern plains there are regions of too high AI to the west and too low AI to the east of the 100th meridian. The bias originates in 1) far too high AI in the interior northwest, 2) AI values that are not low enough in

Annual Mean
NLDAS2
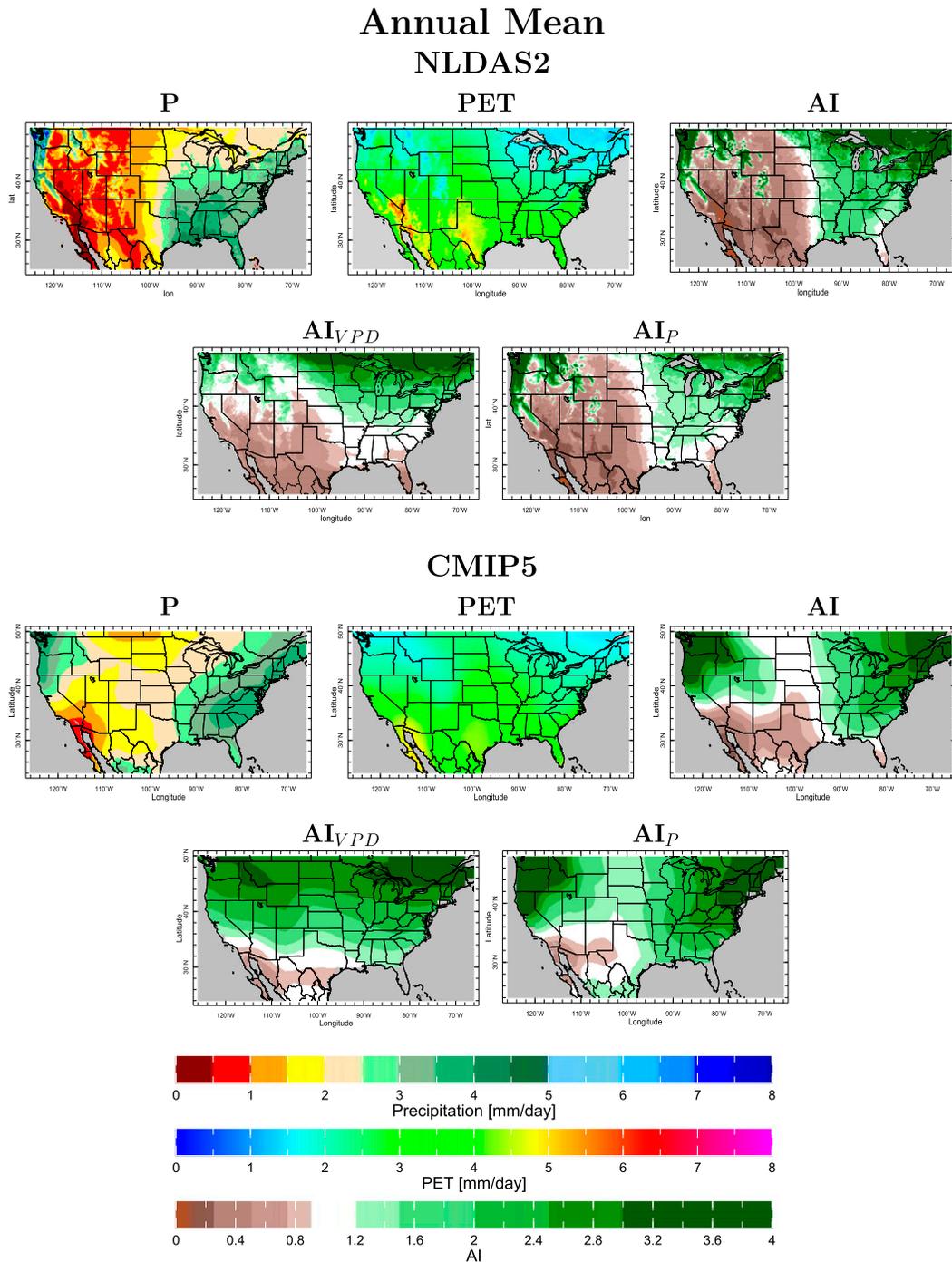
CMIP5

Figure 2. Annual-mean *P*, PET, and AI (top and third rows) and the AI that results from zonal variations in (left) VPD alone (second and bottom rows) and (right) *P* alone (second and bottom rows) for the (top) CMIP5 multimodel average and (bottom) NLDAS-2 evaluated for the same 1979 to 2014 period. Units for *P* and PET are mm day^{-1}.

the western plains at all longitudes and in the southwest, and 3) too weak a gradient of increasing AI from the central to eastern plains (even as the models overestimate AI in the Appalachian region).

Next, as in Part I, we recompute for each model AI while setting all quantities except 1) VPD and 2) P to their zonal-mean values for the season and year and then average across the models. This allows determination of the causes of zonal variations in AI within the model ensemble mean. Figure 2 shows the AI that derives from zonal variations in VPD alone AI_{VPD} and the AI arising from zonal variations in P alone AI_P for both NLDAS-2 and the CMIP5 multimodel mean. Both contribute to the model biases in simulating the AI field. The models underestimate the tendency to aridity introduced by high VPD in southwestern North America and extending into the southern and central plains. Errors in the precipitation simulation make the AI_P too high across the interior northwest, the northern plains, and southwest and southern plains. This is no doubt, in part, because of the low model resolution not representing the topography of the coastal ranges and their ability to wring out moisture. In general, the models underestimate how dry the interior west of North America is. The models also overestimate AI_P in the southeast and Appalachian region.

To examine the relations between model AI, P, and moisture transports, in Figure 3 we plot annual-mean P, actual evapotranspiration E, and $P - E$ for NLDAS-2, ERA-Interim, and the CMIP5 multimodel mean and the vertically integrated moisture transport for ERA-Interim and the multimodel mean. In a steady state, the convergence of the vertically integrated moisture transport balances $P - E$. At the surface, in steady state and the absence of a moisture source for the atmosphere (e.g., oceans and lakes), $P - E$ must be positive and balanced by runoff. Relative to NLDAS-2, the models are too wet across the west and too dry in the Midwest, decreasing the zonal gradient of P. Comparing the ERA-Interim and model moisture transports it is seen that, in the northwest, the models do not simulate the coastal trapping of moisture incoming from the Pacific Ocean by the coastal ranges and instead allow too high precipitation to extend too far inland to the east. Too much moisture also leaks into the interior west from the Pacific Ocean across California and Mexico (see also Sheffield et al. 2013). More generally, the models have excessive P across much of the continent with the exception of the Gulf Coast. This is not attributable, in general and clearly, to erroneous moisture transport from the oceans to the continent, except across western mountains. Instead, the excess P goes along with excess E. Sustaining excess P with excess E allows for less of a bias in $P - E$ (and, hence, runoff), and model $P - E$ compares more favorably with NLDAS-2 $P - E$ than does P or E. (The ERA-Interim $P - E$ is unphysically negative in the western plains and the southwest, which emphasizes the difficulty data assimilation schemes have handling the hydrological cycle.) Regardless, the conclusion is that the models recycle too much moisture between the land surface and precipitation. Excess recycling increases P. If PET was unchanged, increasing P would increase AI. However, too much recycling also causes excess ET and, hence, surface cooling that could reduce PET and further increase AI.

4.2. Bias-corrected model projections of changes in aridity

In Figure 4, we show maps of the bias-corrected AI averaged over 2021–40, 2041–60, 2061–80, and 2081–99 as well as the differences between these periods

Annual Mean

P **E** **P-E, moisture flux (vectors)**
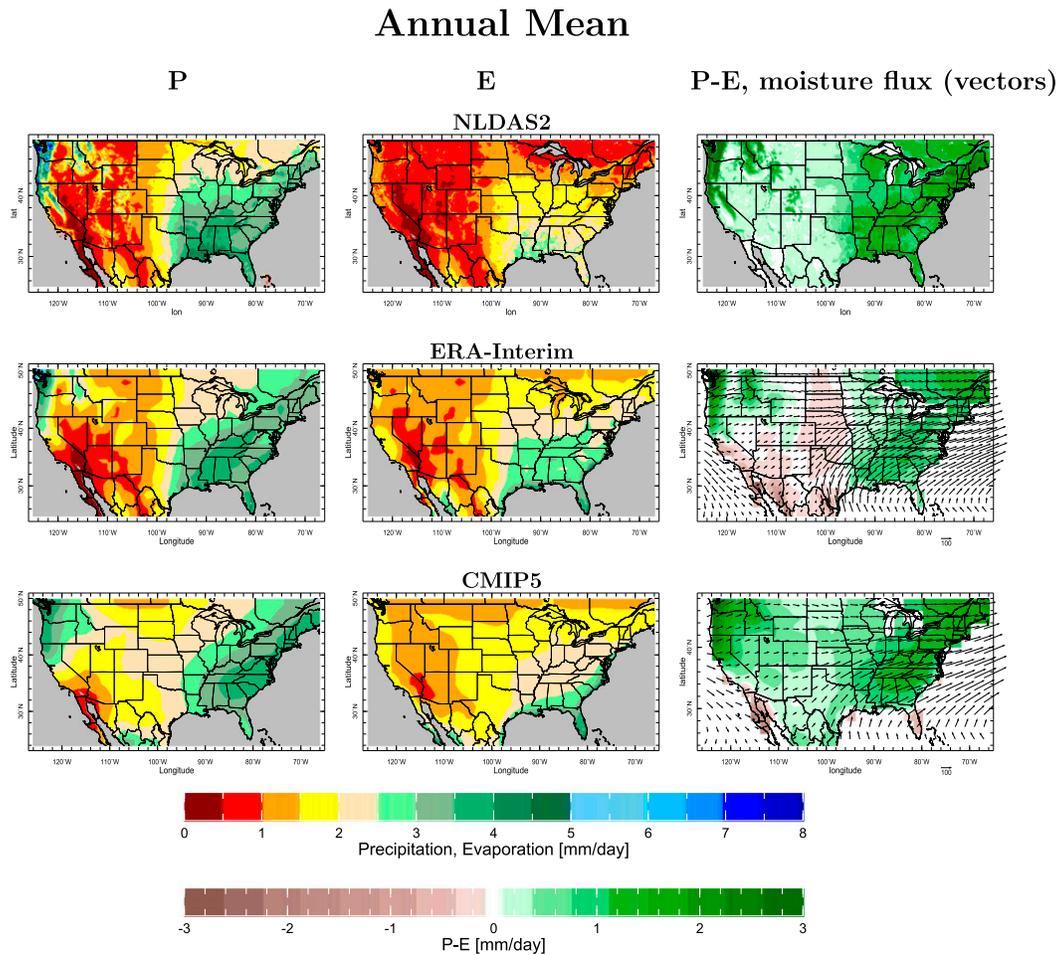
Figure 3. (columns left to right) Annual-mean *P*, *E*, and *P − E* for (top) NLDAS-2, (middle) ERA-Interim, and the (bottom) CMIP5 multimodel mean. For ERA-Interim and CMIP5, the vertically integrated moisture fluxes are also shown as vectors. All results are for 1979 to 2015. The units for *P*, *E*, *P − E* are mm day^{-1}, and the moisture fluxes are kg^{-1} m^{-2} s^{-1} with reference vectors at bottom right of panels

and the 1979–2015 NLDAS-2 AI$_{N,h}$. Notably the essential spatial structure of AI with the marked zonal gradient in the plains remains over the course of the twenty-first century. However, comparing to the 1979–2015 AI map in Figure 3, there is a noticeable eastward encroachment of low AI into the western plains, while the region of AI ≈ 1 moves east across the borders of South Dakota–Minnesota, Nebraska–Iowa, Kansas–Missouri, Oklahoma–Arkansas, and Texas–Louisiana. There is a striking increase in the relative aridity (lower AI) in the Gulf Coast states and Appalachia and parts of the Midwest. This is easily seen in the maps of change in AI, where it is also noticed that AI declines more in the east than in the west of the United States. As such the aridity gradient not only moves eastward but also

Bias Corrected Aridity Index

2021-2040

2041-2060

2061-2080

2081-2099

Bias Corrected Aridity Index - NLDAS2 AI 1979-2015

2021-2040

2041-2060

2061-2080

2081-2099
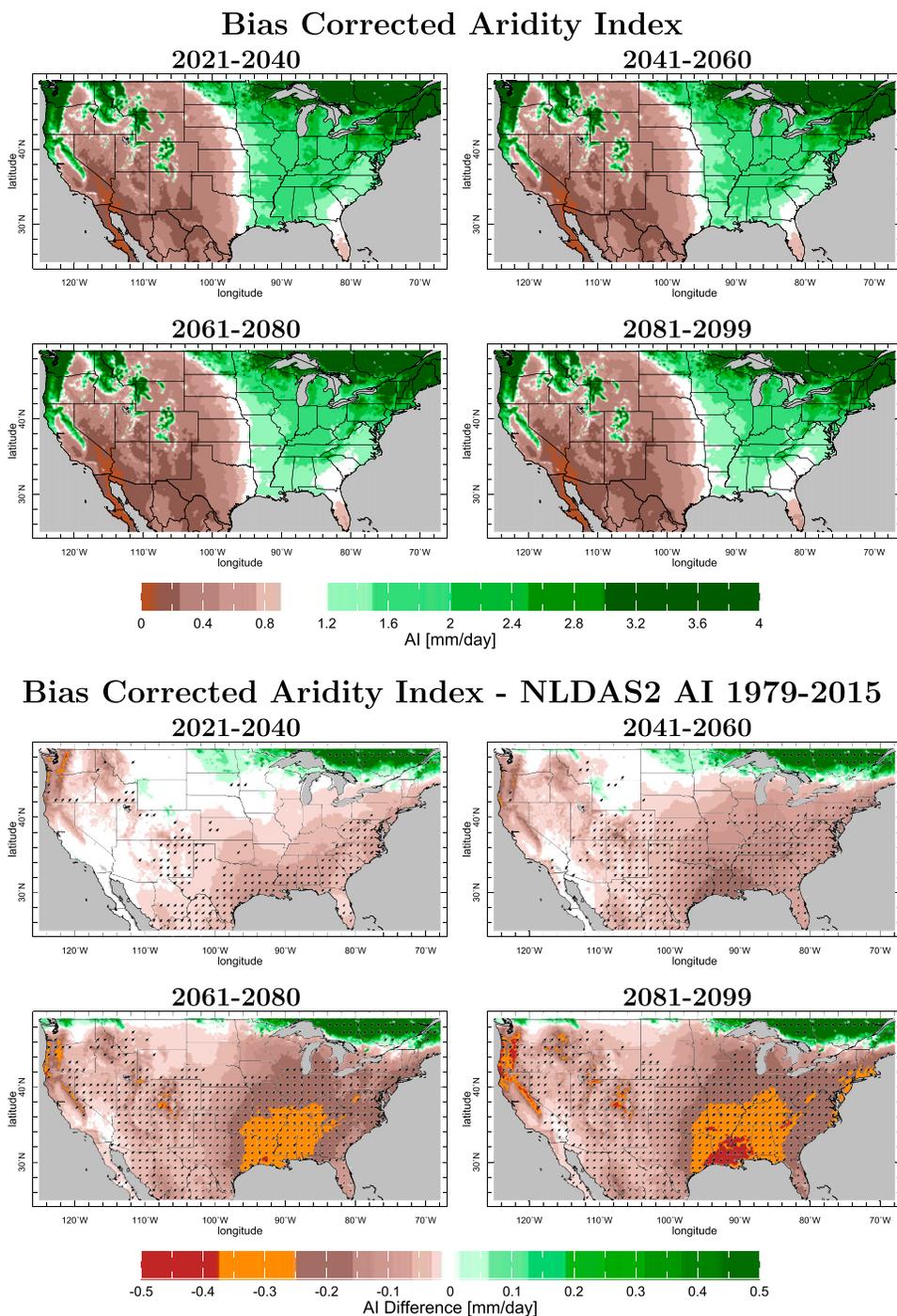
Figure 4. (top) Annual-mean, bias-corrected AI as computed from the CMIP5 model ensemble for four two-decade periods of the current century shown as absolute values and (bottom) difference relative to the 1979–2015 climatological values. In the difference maps, stippling is added where more than three-quarters of the models agree on the sign of the change and agree with the ensemble-mean sign change.

becomes more muted. By midcentury there is widespread model agreement on these changes away from the locations where the projected change is small.

What are the main causes of the change in AI? To examine this we recompute the bias-corrected AI holding, for each model, the PET fixed at the climatological 1979–2015 value but allowing P to change to create $AI_{N,f,P}$ and then allow PET to vary while holding P at the climatological value to create $AI_{N,f,PET}$ (see section 3 for the details). Figures 5 and 6 show the maps of $AI_{N,f,P}$ and $AI_{N,f,PET}$ and their change relative to the historical period $AI_{N,h}$ in the same format as for the total changes in Figure 4.

The changes in P alone tend to reduce AI in the southern part of North America, most strongly in the Gulf states, and increase AI across northern North America, most strongly in the Northeast. There is considerable model agreement on these changes. These patterns are somewhat different to changes in P alone (see Seager et al. 2014) because of the seasonal weighting by PET, which provides preferential weighting to the cooler, low PET, seasons. The P-induced changes in AI only modestly weaken the AI gradient across the southern plains. In contrast, the PET-induced changes in AI cause a notable decline everywhere in Mexico and the United States and also a weakening of the west–east gradient as AI declines more east of the 100th meridian than west (again with considerable model agreement). This is because a given change in PET will yield a larger change in AI in the east, where the historical PET is smaller and the historical AI is larger than in the west. The models agree everywhere that climate change will increase PET and tend to reduce AI. This is no doubt because of the dominant influence of rising temperature and vapor pressure deficit on PET (Cook et al. 2014).

To look at the temporal evolution of the aridity gradient we average the AI over latitude for the northern (42°−48°N), central (36°−42°N), and southern (30°−36°N) plains. The time span covers 1979 to 2100 and so shows the actual NLDAS-2 AI followed by the bias-corrected AI from 2016 on. A time smoothing has been applied primarily to reduce the year-to-year variability that is strong in NLDAS-2. The model projections are an average across models and, in contrast, are relatively smooth in time because of isolating the forced response. The resulting Hovmöller plots are shown in Figure 7. The general decrease in AI is clear at all longitudes as well as the muting of the zonal gradient, while the eastward shift of AI values is most evident in the southern and central plains and less so in the north. Nonetheless, in terms of AI value, the effective 100th meridian progressively moves east as the century advances.[1]

4.3. Potential influences of aridity change on the farm economy

In Part I, we showed maps that demonstrated how farm size, number of farms, rangeland coverage, and percent of cropland used to grow wheat or corn have evolved to reflect the sharp west–east aridity gradient across the plains, albeit with notable exceptions (e.g., Nebraska where irrigation from the Ogallala Aquifer allows cultivation of corn in a dry state). Here, we present the same data in a

---

[1] We also evaluated the variability of annual-mean AI values. Relative to NLDAS-2, the average of variability across the models reasonably reproduces interannual variability of AI in the plains but underestimates it in the northern plains. The models do not project a notable change in AI variability over the current century.

Bias Corrected $\text{AI}_{N,f,P}$

2021-2040

2041-2060

2061-2080

2081-2099

Bias Corrected $\text{AI}_{N,f,P}$ - NLDAS2 AI 1979-2015

2021-2040

2041-2060

2061-2080

2081-2099
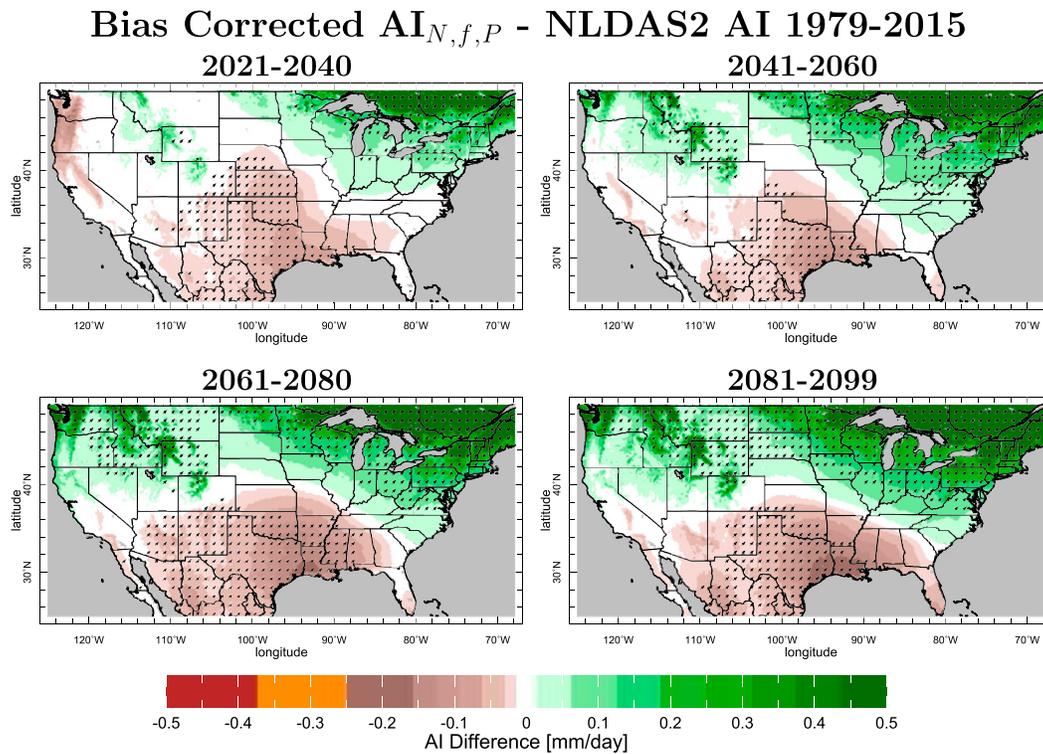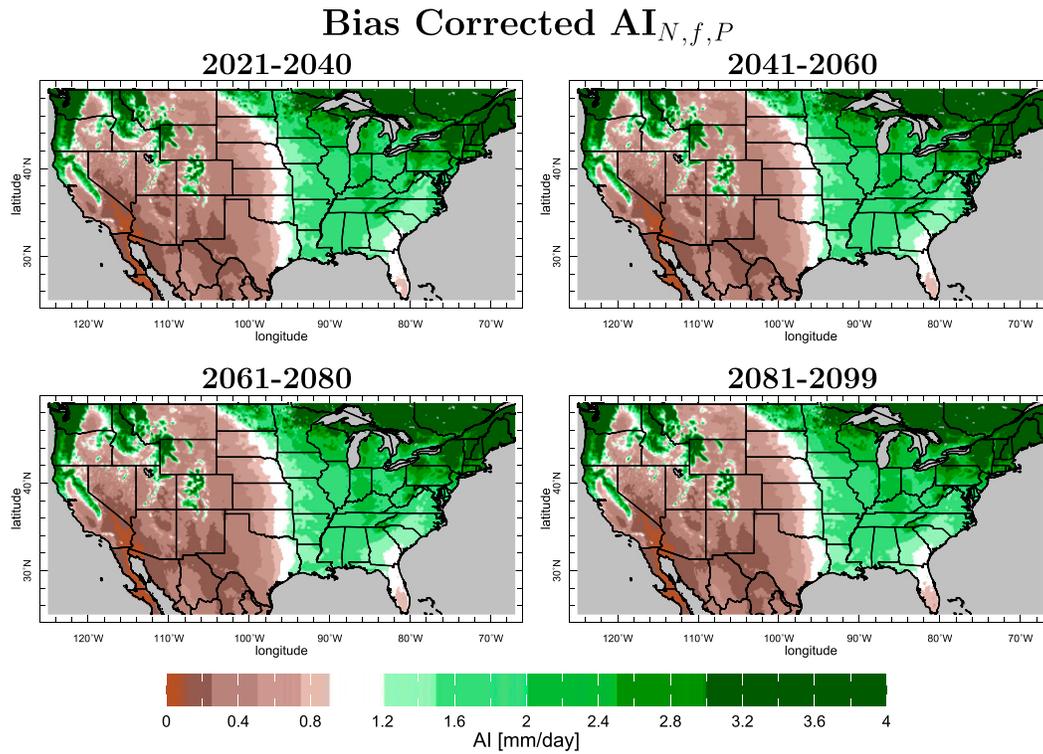
Figure 5. As in **Figure 4**, but only allowing *P* to change, keeping PET at the 1979–2015 climatological values.

Bias Corrected $AI_{N,f,PET}$

2021-2040   2041-2060

2061-2080   2081-2099

Bias Corrected $AI_{N,f,PET}$ - NLDAS2 AI 1979-2015

2021-2040   2041-2060

2061-2080   2081-2099
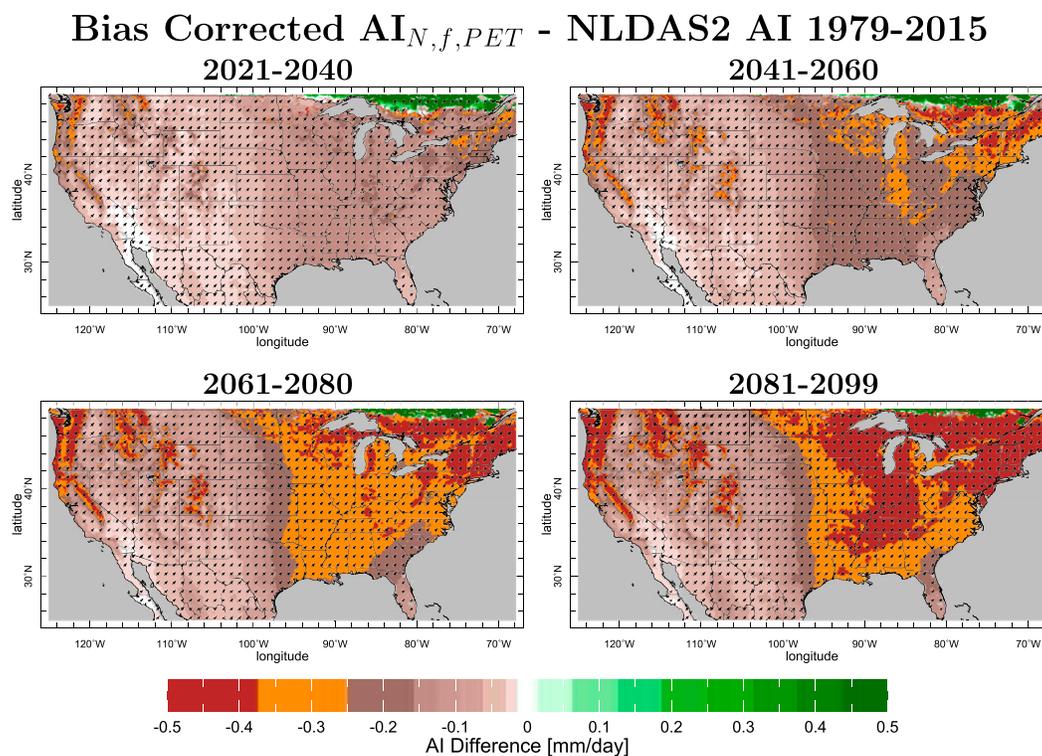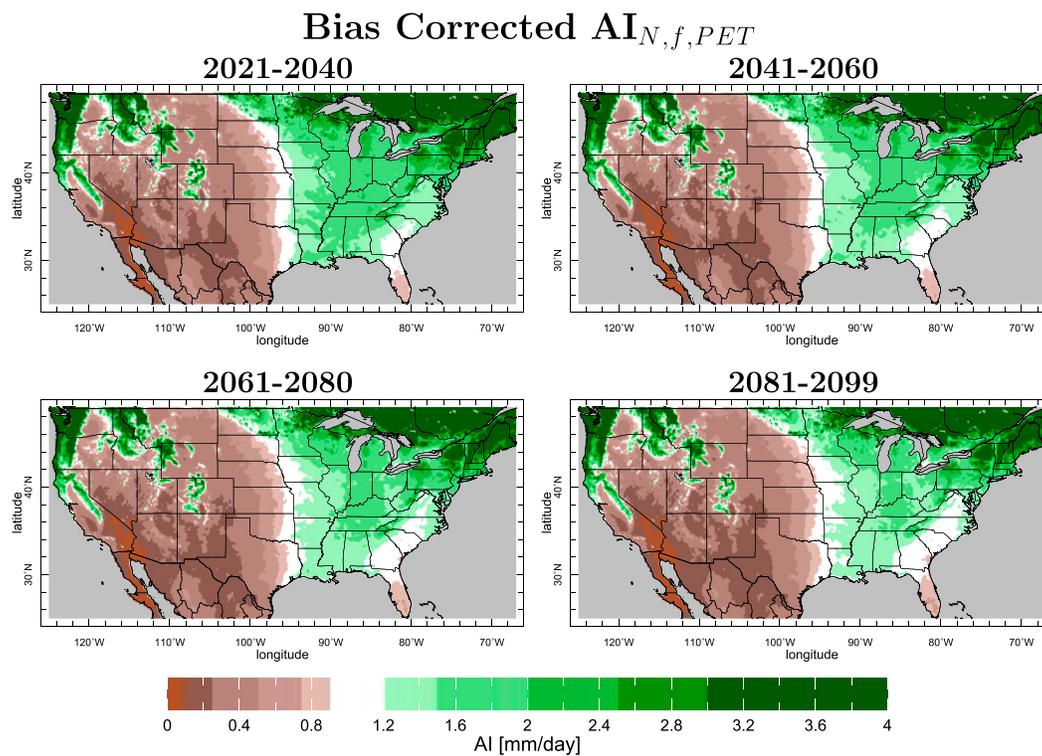
Figure 6. As in **Figure 4**, but only allowing PET to change, keeping *P* at the 1979–2015 climatological values.

Plains Aridity Index NLDAS2 and CMIP5

(a) Northern

(b) Central
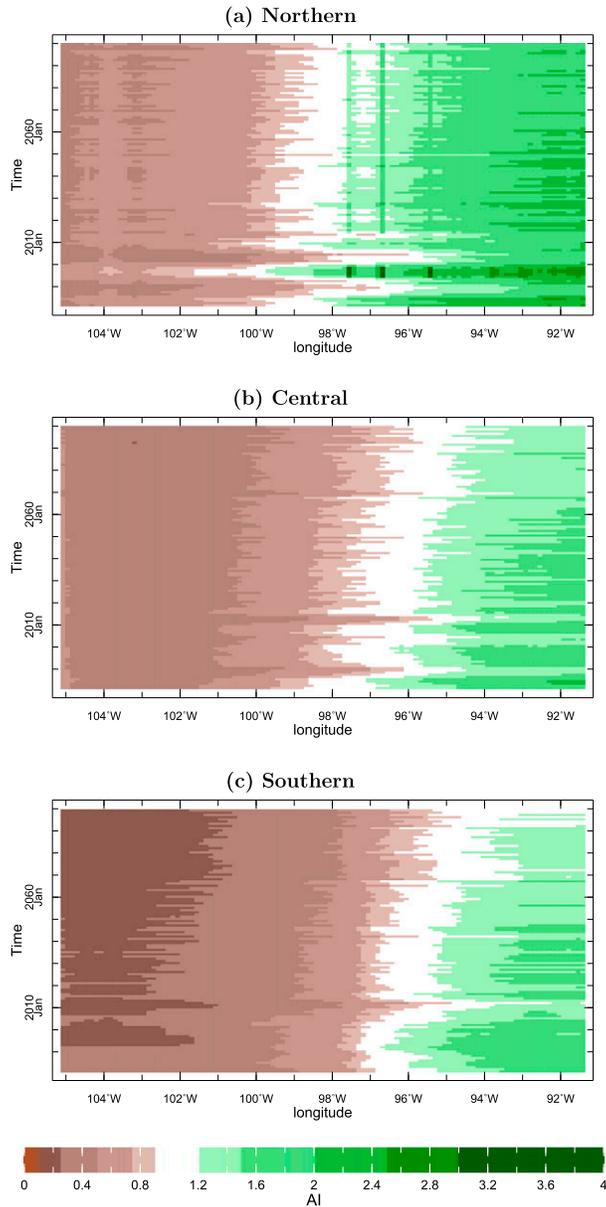
(c) Southern

Figure 7. The NLDAS-2 AI for 1979–2015 followed by, for 2016–2099, the bias-corrected AI as computed from the CMIP5 model ensemble and averaged over the (top) northern, (middle) central, and (bottom) southern plains as a function of time (vertical axis) and longitude (horizontal axis).

different way by plotting in Figure 8, for the northern, central, and southern plains, the farm size, percent of the county under rangeland, and percent of cropland under corn as a function of the NLDAS-2 AI. Each data point is the average across latitude and longitude for a 1° longitudinal bin.
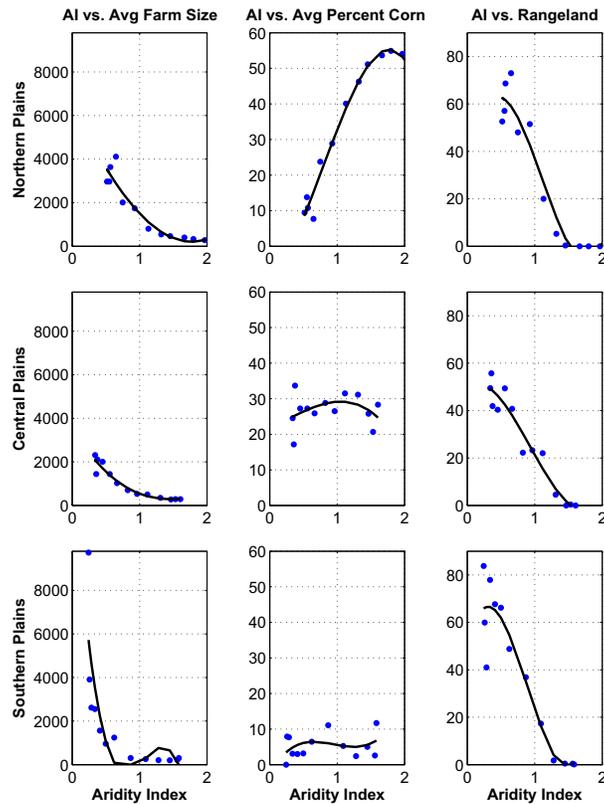
Figure 8. (left)The farm size in acres, (center) percent of cropped land under corn, and (right) average percent of counties under rangeland plotted against the 1979–2015 AI from NLDAS-2 for the (top) northern, (middle) central, and (bottom) southern plains. The values corresponding to the dots are the average for 1° longitude bins. The black lines are best-fitting, third-order polynomial curves.

To assess how the projected changes in AI might impact the farm economy, we will use statistical relations described by the third-order polynomial curves that best fit the observed farm variable–AI relations. These curve fits are also shown in Figure 8 for the three farm quantities and three regions of the plains. Consistent with the maps shown in Part I, at all latitudes there is a decrease in farm size as AI increases. This is the reflection in farm–AI space of the decrease in farm size from west to east across the plains, as expected in terms of the area of operation required to achieve profitability in the face of lower aridity and increased land productivity. In the southern and central plains, there is little relation between the percent of cropped land under corn and AI. This reflects the small area under corn in the south and the "Nebraska exception"—high percentage of corn cropping in an arid area caused by accessible groundwater and irrigation—in the central plains. However, in the northern plains there is a clear increase of the percent of cropped land under corn as AI increases, reflecting the transition from wheat cultivation in the northwest plains to corn cultivation in the northeast plains (see Part I).

Across the plains the percent of counties under rangeland decreases from west to east, reflecting the opportunity for more intensive use of land in the more humid eastern plains.

The bias-corrected projections of AI can then be used to infer from the curves in Figure 8 the projected future changes in farm size and percent of cropped land under corn. That is, we first develop the current functional relations: $FS_h = p(AI_{N,h})$, $PC_h = q(AI_{N,h})$, $PR_h = r(AI_{N,h})$, where FS_h is current farm size, PC_h is current percent cropped land under corn, PR_h is current percent county under rangeland, and p, q, r are the polynomial functions in Figure 8. The projections are then $FS_f = p(AI_{N,f})$, $PC_f = q(AI_{N,f})$, $PR_f = r(AI_{N,f})$. Figure 9 then shows the farm size, percent cropped land under corn, and percent county under rangeland as a function of longitude for the present and two-decade periods during the current century. The varying strength of the dependence of farm size on AI introduces interesting latitudinal structure to the projections of increase in farm size. While AI decreases most in the southeastern plains (where farm size is projected to increase), the largest increase in farm size is projected for the southwestern plains because here, while the decrease in AI is smaller, the historical relation between decreasing AI and increasing farm size is very strong (Figure 8). In the southwestern plains, this naive model would suggest farms will need to increase their size by a quarter to a third to restore equilibrium with the increased aridity. In the central and northern plains, the decrease in AI is less, and the sensitivity of farm size to is AI weaker, and these combine to give consistent but modest projections of increases in farm size on the order of 10%.

As expected for the southern and central plains the changes in AI do not lead to projected changes in the percent of cropped land under corn because of the absence of dependence of the latter on AI or longitude in the historical period. In the northern plains, where the U.S. Corn Belt encroaches in the east and corn can reach over 50% of cropped land, declining AI leads to little change in the percent of corn in the near future but a decline of up to a few percent later in the century. Although not shown, the same methodology projects that wheat cropping would expand in the cropland vacated by corn. In all regions of the plains, and primarily east of the 100th meridian, the naive model suggests an increase in the percent of land under rangeland as aridity increases.

5. Discussion and conclusions

The 100th meridian was shown in Part I to be a stark divider between a more arid west and more humid east that is expressed well in the natural landscape and also in the farm economy. While the plains have experienced a never-ending variation between times of drought and times of pluvial (Cook et al. 2007; Stahle et al. 2007; Seager et al. 2005; Herweijer et al. 2006; Schubert et al. 2004; Forman et al. 2001) in which the aridity gradient would have changed in intensity and location, it appears that agriculture has evolved in a way that the size of farms, and how the farm land is used, responds to the mean aridity gradient. However, in recent decades, human-induced climate change has been added onto this natural variability. The United States has broadly warmed (apart from the southeast; Capparelli et al. 2013), while radiatively forced precipitation changes have been modest to date (with a slight reduction in the southwest; Seager and Hoerling 2014). Consequently, we argue that the farm economy has come into rough statistical equilibrium with the spatially varying aridity
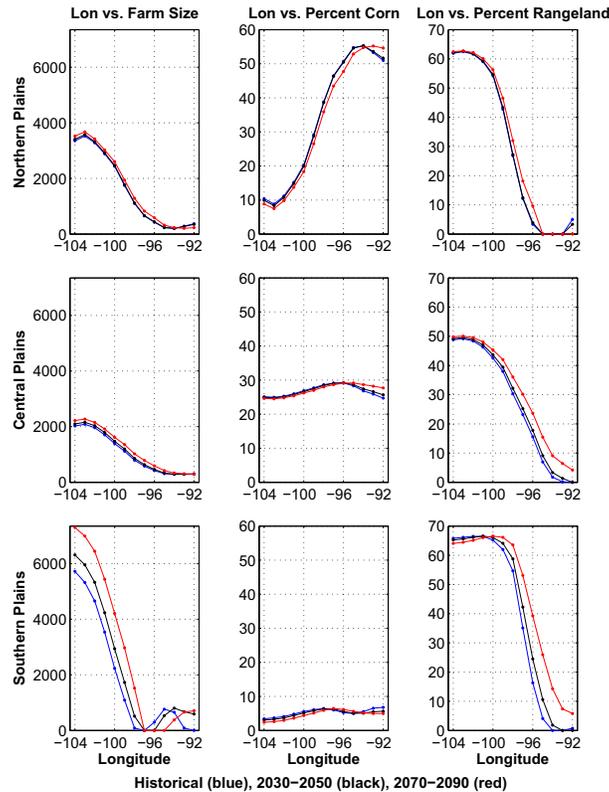
Figure 9. (left) The farm size in acres, (middle) projected percent of cropped land under corn, and (right) percent of land under rangeland plotted against longitude for the (top) northern, (middle) central, and (bottom) southern plains and for 1979–2005 (blue) and projected 2030–50 (black) and 2070–90 (red). The projections use the best-fit curves to the historical relation between farm variables and AI and the bias-corrected AI from CMIP5 models.

intensity of the plains and the oscillations between drier and wetter years. This reasoning also implies that the farm economy will evolve as the climate conditions of the plains respond to rising greenhouse gases. To determine what might happen requires projections by models of future conditions. This in turn requires an assessment of how well models can simulate the aridity intensities of the plains. In this paper we assess the ability of the current generation of state-of-the-art climate models that participated in CMIP5 to simulate North American climate, focusing on the plains, and also develop statistical relations between aspects of the farm economy and aridity. Finally, we develop bias-corrected projections of aridity and use these to develop simple projections of the farm economy variables over the current century. The conclusions are as follows:

(i) Climate models generally fail to correctly simulate the amplitude and spatial variation of aridity, measured by $AI = P/PET$, across North America. While they tend to have reasonably realistic PET, which is

primarily influenced by temperature, they tend to overestimate *P* because of excessive continental *E* and are unable to simulate the trapping of wintertime eastward moisture advection from the Pacific by the coastal ranges. As such, the models overestimate AI, underestimate its gradient across the plains, and fail to demarcate the stark contrast across the continent between an arid west and a humid east with the 100th meridian as the well-defined, semiarid, subhumid border.

(ii) To preserve the gradient in the projections of AI we developed a bias-corrected method that altered the observations-based AI from NLDAS-2 by the fractional difference between the CMIP5 multimodel means for the future and the 1979–2015 historical period. The bias-corrected projections show an overall decrease in AI (increase in aridity) across Mexico and the United States.

(iii) When the model projections of future AI are decomposed into contributions from changes in *P* and PET it is shown that the change in *P* causes increased aridity across southern North America and decreased aridity to the north but that rising PET (caused by atmospheric warming) causes increasing aridity everywhere.

(iv) Because of the greater AI and smaller PET in the east than the west, the projected cross-continent increases in PET cause aridity to increase by more in the east than the west. This reduces the strength of the west–east aridity gradient across the central part of the continent. It also means that the effective 100th meridian—that defined by an aridity level as opposed to a specific longitude—moves progressively east as the century progresses.

(v) Aspects of the farm economy well reflect the west–east aridity gradient. Across the plains, farm size increases as aridity intensifies (to the west). In the northern plains, as aridity declines from west to east, cropped land is increasingly used to grow corn instead of wheat. Given the reasonable assumption that the farm economy evolved over the past century and more to adjust to the environmental conditions, it is expected that it will evolve further in coming decades as those environmental conditions progressively change toward heightened aridity. A simple projection of the current farm economy–AI relations into the future predicts that farm size will need to increase across the plains, but especially in the south, and that in the northern plains there will be a shift toward wheat cultivation and away from corn. Rangeland would expand to the east. The changes in farm size and percent of cropland under wheat or corn are coupled. The value of production and profit per acre are higher for corn than for wheat (see USDA data at https://www.ers.usda.gov/data-products/commodity-costs-and-returns/), and hence a shift from corn to wheat will require an increase in farm size to maintain farm profitability. Across the plains but primarily east of the 100th meridian the projections suggest increased percent of land under rangeland. The current west–east gradients in farm size, choice of crop, and rangeland already reflect environmental reality, and so the projected environmental-driven changes make sense, all else being equal.

There are many caveats that should be attached to this work and its conclusions. First, we have shown that state-of-the-art models simulate the aridity gradient

across North America poorly. Hence, even though we have applied a bias correction to the projections to remove the mean state bias, it can be questioned whether these models should be trusted to properly simulate the changes. In response we would say that the model error that leads to an incorrect mean state aridity arises from the precipitation simulation, while the projected aridity change arises most strongly from the temperature and vapor pressure deficit change, which we suspect is more faithfully simulated. Second, while current Earth system models (the subset of all climate models that simulate, in varying degrees of complexity, vegetation and carbon dynamics) predict widespread declines in soil moisture and increases in continental aridity, they also simulate increases in net primary productivity (Scheff et al. 2017; Mankin et al. 2017). This is because, within the models, the beneficial effects on photosynthesis and water-use efficiency of increased CO_2 overwhelm the effects of increased temperature and vapor pressure deficit. Hence, perhaps, the aridity gradient as expressed in vegetation and crops will not move east as suggested here on the basis of a simple metric like AI in which the computation of PET does not account for biophysical changes. In response, we would say that CO_2 effects thus far appear to be highly geographically variable (Zhu et al. 2016) and that models quite conceivably overestimate the biophysical response to CO_2 [see review by Cook et al. (2016) and discussions in Scheff et al. (2017), Mankin et al. (2017), and Allen et al. (2015)]. However, it is also likely that enhanced CO_2 is increasing crop water-use efficiency to some degree and may alter the relationship between the farm economy and AI. Third, the farm economy projections do not account for changes in crop technology, farming practice, farm policy, and the wider economy. In response we would say that this is an entirely valid criticism, and we emphasize that the farm projections are ''naive'' and merely attempt to illustrate how, all else being equal, the farm economy would adjust to future changes in AI, given how it has adjusted to prevailing AI over past decades. That said, complex calculations that use a computable general equilibrium model of the U.S. farm economy driven by climate model projections (Malcolm et al. 2012) also conclude that there will be a shift from corn to wheat in the area that our naive methods project the same transition. However, the projected expansion of rangelands eastward may be restricted because this is into lower regions with higher daytime maximum and nighttime minimum temperatures that could stress cattle (e.g., Gaughan et al. 2010).

Over the past century the adjustment of the farm economy to aridity in the plains was not steady but instead occurred in jumps. The Dust Bowl drought of the 1930s made evident that many farms were too small to ensure profitability in the face of adverse environmental conditions and to effectively practice erosion control (Hansen and Libecap 2004). Recovery from the drought led to a permanent increase in farm size and a permanent change in many aspects of the agricultural economy (Hornbeck 2009). The steady increase in aridity over the current century shown here is also artificial. It is only that steady because we have averaged across many different climate models in order to identify the common change caused by rising greenhouse gases. In the real world, the response to radiative forcing will occur against the background of natural variability on interannual to decadal time scales. Variability plus forced change can combine to create abrupt shifts in aridity or temporally mask an ongoing forced aridification. Advances in decadal prediction of the natural variability of oceans and their influence on North American

hydroclimate (Seager and Ting 2017) and projection of forced change might allow anticipation of how the natural environment of the plains will alter over the coming decades. This information may be able to inform policy that can aid adaptation to changing conditions and avoid the negative effects of surprises followed by crises and social and economic disruption.

REFERENCES

Allen, C. D., D. D. Breshears, and N. G. McDowell, 2015: On underestimation of global vulnerability to tree mortality and forest die-off from hotter drought in the Anthropocene. *Ecosphere*, **6**, 1–55, https://doi.org/10.1890/ES15-00203.1.

Allen, R. G., L. S. Pereira, D. Raes, and M. Smith, 1998: Crop evapotranspiration—Guidelines for computing crop water requirements—FAO Irrigation and drainage. Food and Agricultural Organization of the United Nations Irrigation and Drainage Paper 56, 333 pp.

Capparelli, V., C. Franzke, A. Vecchio, M. P. Freeman, N. W. Watkins, and V. Carbone, 2013: A spatiotemporal analysis of U.S. station temperature trends over the last century. *J. Geophys. Res. Atmos.*, **118**, 7427–7434, https://doi.org/10.1002/jgrd.50551.

Cook, B. I., J. E. Smerdon, R. Seager, and S. Coats, 2014: Global warming and 21st century drying. *Climate Dyn.*, **43**, 2607–2627, https://doi.org/10.1007/s00382-014-2075-y.

——, T. R. Ault, and J. E. Smerdon, 2015: Unprecedented 21st century drought risk in the American Southwest and central plains. *Sci. Adv.*, **1**, e1400082, https://doi.org/10.1126/sciadv.1400082.

——, E. R. Cook, J. E. Smerdon, R. Seager, A. P. Williams, S. Coats, D. W. Stahle, and J. Villaneuva Diaz, 2016: North American megadroughts in the Common Era: Reconstructions and simulations. *Wiley Interdiscip. Rev.: Climate Change*, **7**, 411–432, https://doi.org/10.1002/wcc.394.

Cook, E. R., R. Seager, M. A. Cane, and D. W. Stahle, 2007: North American droughts: Reconstructions, causes, and consequences. *Earth-Sci. Rev.*, **81**, 93–134, https://doi.org/10.1016/j.earscirev.2006.12.002.

Daly, C., W. P. Gibson, G. H. Taylor, G. L. Johnson, and P. Pasteris, 2000: High-quality spatial climate data sets for the United States and beyond. *Trans. Amer. Soc. Agric. Biol. Eng.*, **43**, 1957–1962, https://doi.org/10.13031/2013.3101.

Dee, D., and Coauthors, 2011: The ERA-Interim reanalysis: Configuration and performance of the data assimilation system. *Quart. J. Roy. Meteor. Soc.*, **137**, 553–597, https://doi.org/10.1002/qj.828.

Forman, S., R. Oglesby, and R. S. Webb, 2001: Temporal and spatial patterns of Holocene dune activity on the Great Plains of North America: Megadroughts and climate links. *Global Planet. Change*, **29**, 1–29, https://doi.org/10.1016/S0921-8181(00)00092-8.

Gaughan, J. B., T. L. Mader, S. M. Holt, M. L. Sullivan, and G. L. Hahn, 2010: Assessing the heat tolerance of 17 beef cattle genotypes. *Int. J. Biometeor.*, **54**, 617–627, https://doi.org/10.1007/s00484-009-0233-4.

Hansen, Z. K., and G. D. Libecap, 2004: Small farms, externalities, and the Dust Bowl of the 1930s. *J. Political Econ.*, **112**, 665–694, https://doi.org/10.1086/383102.

Herweijer, C., R. Seager, and E. R. Cook, 2006: North American droughts of the mid to late nineteenth century: History, simulation and implications for mediaeval drought. *Holocene*, **16**, 159–171, https://doi.org/10.1191/0959683606hl917rp.

Hornbeck, R., 2009: The enduring impact of the American Dust Bowl: Short- and long-run adjustments to environmental catastrophe. National Bureau of Economic Research Tech. Rep. Working Paper 15605, 40 pp.

Malcolm, S., E. Marshall, M. Aillery, P. Heisey, M. Livingston, and K. Day-Rubenstein, 2012: Agricultural adaptation to a changing climate: Economic and environmental implications vary by U.S. region. U.S. Department of Agriculture Economic Research Rep. ERR-136, 84 pp.

Maloney, E. D., and Coauthors, 2014: North American climate in CMIP5 experiments: Part III: Assessment of 21st century projections. *J. Climate*, **27**, 2230–2270, https://doi.org/10.1175/JCLI-D-13-00273.1.

Mankin, J. S., J. E. Smerdon, B. I. Cook, A. P. Williams, and R. Seager, 2017: The curious case of projected twenty-first-century drying but greening in the American West. *J. Climate*, **30**, 8689–8710, https://doi.org/10.1175/JCLI-D-17-0213.1.

Mesinger, F., and Coauthors, 2006: North American Regional Reanalysis. *Bull. Amer. Meteor. Soc.*, **87**, 343–360, https://doi.org/10.1175/BAMS-87-3-343.

Powell, J. W., 1879: Report on the lands of the arid regions of the United States, with a more detailed account of the lands of Utah. Government Printing Office, 207 pp.

——, 1890: The irrigable lands of the arid region. *Cent. Mag.*, **39**, 766–776.

Scheff, J., R. Seager, H. Liu, and S. Coats, 2017: Are glacials dry? Consequences for paleoclimatology and for greenhouse warming. *J. Climate*, **30**, 6593–6609, https://doi.org/10.1175/JCLI-D-16-0854.1.

Schubert, S. D., M. J. Suarez, P. J. Pegion, R. D. Koster, and J. T. Bacmeister, 2004: Causes of long-term drought in the U.S. Great Plains. *J. Climate*, **17**, 485–503, https://doi.org/10.1175/1520-0442(2004)017<0485:COLDIT>2.0.CO;2.

Seager, R., and N. Henderson, 2013: Diagnostic computation of moisture budgets in the ERA-Interim reanalysis with reference to analysis of CMIP-archived atmospheric model data. *J. Climate*, **26**, 7876–7901, https://doi.org/10.1175/JCLI-D-13-00018.1.

——, and M. P. Hoerling, 2014: Atmosphere and ocean origins of North American drought. *J. Climate*, **27**, 4581–4606, https://doi.org/10.1175/JCLI-D-13-00329.1.

——, and M. Ting, 2017: Decadal drought variability over North America: Mechanisms and predictability. *Curr. Climate Change Rep.*, **3**, 141–149, https://doi.org/10.1007/s40641-017-0062-1.

——, Y. Kushnir, C. Herweijer, N. Naik, and J. Velez, 2005: Modeling of tropical forcing of persistent droughts and pluvials over western North America: 1856–2000. *J. Climate*, **18**, 4065–4088, https://doi.org/10.1175/JCLI3522.1.

——, M. Ting, C. Li, N. Naik, B. Cook, J. Nakamura, and H. Liu, 2013: Projections of declining surface water availability for the southwestern U.S. *Nat. Climate Change*, **3**, 482–486, https://doi.org/10.1038/nclimate1787.

——, D. Neelin, I. Simpson, H. Liu, N. Henderson, T. Shaw, Y. Kushnir, and M. Ting, 2014: Dynamical and thermodynamical causes of large-scale changes in the hydrological cycle over North America in response to global warming. *J. Climate*, **27**, 7921–7948, https://doi.org/10.1175/JCLI-D-14-00153.1.

Sheffield, J., and Coauthors, 2013: North American climate in CMIP5 experiments. Part I: Evaluation of historical simulations of continental and regional climatology. *J. Climate*, **26**, 9209–9245, https://doi.org/10.1175/JCLI-D-12-00592.1.

Stahle, D. W., F. K. Fye, E. R. Cook, and R. D. Griffin, 2007: Tree-ring reconstructed megadroughts over North America since A.D. 1300. *Climatic Change*, **83**, 133–149, https://doi.org/10.1007/s10584-006-9171-x.

Stegner, W., 1954: *Beyond the Hundredth Meridian.* Penguin Books, 496 pp.

Xia, Y., and Coauthors, 2012a: Continental-scale water and energy flux analysis and validation for the North American Land Data Assimilation System project phase 2 (NLDAS-2): 1. Intercomparison and application of model products. *J. Geophys. Res.*, **117**, D03109, https://doi.org/10.1029/2011JD016048.

——, and Coauthors, 2012b: Continental-scale water and energy flux analysis and validation for North American Land Data Assimilation System project phase 2 (NLDAS-2): 2. Validation of model-simulated streamflow. *J. Geophys. Res.*, **117**, D03110, doi:10.1029/2011JD016051.

Zhu, Z., and Coauthors, 2016: Greening of the Earth and its drivers. *Nat. Climate Change*, **6**, 791–795, https://doi.org/10.1038/nclimate3004.